Carbon cycle response to temperature overshoot beyond 2 °C – an analysis of CMIP6 models

I. Melnikova[1,2], O. Boucher[1], P. Cadule[1], P. Ciais[3], T. Gasser[4], Y. Quilcaille[4], H. Shiogama[2], K. Tachiiri[2,5], T. Yokohata[2] and K. Tanaka[2,3]

[1] Institut Pierre-Simon Laplace, Sorbonne Université / CNRS, France

[2] Center for Global Environmental Research (CGER), National Institute for Environmental Studies (NIES), Japan

[3] Laboratoire des Sciences du Climat et de l'Environnement (LSCE), Commissariat à l'énergie atomique et aux énergies alternatives (CEA CNRS UVSQ), Gif-sur-Yvette, France

[4] International Institute for Applied Systems Analysis (IIASA), Austria

[5] Research Institute for Global Change, Japan Agency for Marine-Earth Science and Technology, Japan

[*]Corresponding author: Irina Melnikova (irina.melnikova@ipsl.fr)

Key Points:

- After a peak of CO_2 growth rate in the SSP5-3.4-OS scenario, land and ocean take up carbon for at least 50 years but at a decreasing rate
- The land sink decrease is due to the larger growth of respiration than photosynthetic production and concurrent land-use change emissions
- Under declining emissions, both land and ocean continue to take up carbon at an asymmetrically larger rate

Abstract

There is a substantial gap between the current emissions of greenhouse gases and levels required for achieving the 2 and 1.5 °C temperature targets of the Paris Agreement. Understanding the implications of a temperature overshoot is thus an increasingly relevant research topic. Here we explore the carbon cycle feedbacks over land and ocean in the SSP5-3.4-OS overshoot scenario by using an ensemble of Coupled Model Intercomparison Project 6 Earth system models. Models show that after the CO_2 concentration and air temperature peaks, land and ocean are decreasing carbon sinks from the 2040s and become sources for a limited time in the 22nd century. The decrease in the carbon uptake precedes the CO_2 concentration peak. The early peak of the ocean uptake stems from its dependency on the atmospheric CO_2 growth rate. The early peak of the land uptake occurs due to a larger increase in ecosystem respiration than the increase in gross primary production, as well as due to a concomitant increase in land-use change emissions primarily attributed to the wide implementation of biofuel croplands. The carbon cycle feedback parameters amplify after the CO_2 concentration and temperature peaks, so that land and ocean absorb more carbon per unit change in the atmospheric CO_2 change (stronger negative feedback) and lose more carbon per unit temperature change (stronger positive feedback) compared to if the feedbacks stayed unchanged. The increased negative CO_2 feedback outperforms the increased positive climate feedback. This feature should be investigated under other scenarios and reflected in simple climate models.

Plain Language Summary

A large gap between required and currently planned greenhouse gas emission reductions makes possible overshooting the 2 °C target of the Paris Agreement before the temperature can return below the target levels. We explore the response of the global carbon cycle to overshoot by

analyzing the simulations of state-of-art models under an overshoot pathway, where the emissions increase until the 2030s and exhibit a steep reduction thereafter. The land and ocean continue to take up carbon from the atmosphere throughout the 21st century, albeit at a reduced rate. The decrease in the ocean carbon uptake occurs before the CO_2 concentration peak due to its dependence on the rate of the atmospheric CO_2 change, and the decrease in the land uptake occurs due to a stronger increase in the ecosystem respiration than in the photosynthetic carbon absorption and simultaneous large land-use-change emissions from the expansion of biofuel crops. After the peaks, land and ocean absorb more carbon from the atmosphere due to higher CO_2 concentration and lose more carbon due to warmer temperatures. The influence of higher CO_2 concentration wins over the influence of warming, allowing land and ocean to remain carbon sinks till the end of the 21st century.

1 Introduction

The Paris Agreement aims for a long-term temperature target of holding global temperature increase below 2 °C and pursuing efforts to keep warming to no more than 1.5 °C (UNFCCC, 2015). However, there is a substantial gap between the required mitigation efforts to achieve this ambitious target and planned national policies towards emissions reductions. According to the Intergovernmental Panel on Climate Change (IPCC) Special Report "Global warming of 1.5 °C", achieving the temperature target without an overshoot, i.e., temporarily exceeding the 1.5 or 2 °C limits, requires a rapid decline in global net anthropogenic CO_2 emissions by 2030 up to 45% for the 1.5 °C and up to 25% for the 2.0 °C targets. On the one hand, more than 100 countries have adopted or planned to adopt net-zero targets by the year 2050, and China, which is currently the largest emitter of greenhouse gases (GHGs), promised to become carbon neutral before 2060 (Mallapaty, 2020). On the other hand, current nationally

determined contributions indicate a slight increase in the CO_2 emissions in 2030 compared to 2020 levels meaning that current emission pledges may not be enough to achieve the Paris Agreement temperature targets (Höhne et al., 2020). Based on the assessment of current policies, Hausfather & Peters (2020) showed that global warming is on course to exceed 3 °C by the end of this century. Consequently, the possibility of temperature overshoot should be considered by the scientific community.

Our current understanding of the consequences of a temperature overshoot on the carbon cycle is limited. Several studies analyzed the carbon cycle feedbacks in the land and ocean under overshoot scenarios (Boucher et al., 2012; Jones et al., 2016a; Zickfeld et al., 2016; Palter et al., 2018; Schwinger & Tjiputra, 2018; Tokarska et al., 2019; Jeltsch-Thömmes et al., 2020). Using idealized ramp-up and ramp-down scenarios (with increasing and later decreasing CO_2 concentration at a 1% $year^{-1}$ rate) Boucher et al. (2012) and Zickfield et al. (2016) showed that land continues to act as a carbon sink for a long time after the temperature overshoots, while the ocean turns into a source only a few decades after the ramp-down starts. Palter et al. (2018) considered an overshoot scenario, where CO_2 concentration increases until 2060, following a Representative Concentration Pathway (RCP8.5), and rapidly decreases after. They showed that both land and ocean become a carbon source nearly two to three decades after the peaks of CO_2 concentration and temperature. Schwinger & Tjiputra (2018) found that the ocean turns into a carbon source only after a strong reduction in atmospheric CO_2 because the disequilibrium in the sea-air partial pressure is maintained for a long time after the peak of CO_2 concentration. The bottom line is that existing studies all agree that land and ocean act as decreasing sinks at least for a couple of decades after the ramp-down starts, but it is difficult to assess the robustness of the other findings of these studies. Indeed, the studies are based on different, highly idealized

scenarios. They also consider a limited number of models, and some of these models are of intermediate complexity with little traceability to more complex models in the context of overshoot scenarios. Thus, the role of more complex processes controlling the response of the carbon cycle to the overshoot of the Paris Agreement temperature target remains largely unexplored.

The response of the carbon cycle to the changes in the atmospheric CO_2 concentrations and climate can be characterized by the carbon cycle feedback framework via carbon-concentration (β) and carbon-climate (γ) feedback parameters, respectively (Friedlingstein et al., 2006; Gregory et al., 2009; Jones et al., 2016b; Schwinger & Tjiputra, 2018; Williams et al., 2019; Arora et al., 2020; Jones & Friedlingstein, 2020). An application of these carbon cycle feedback metrics to an overshoot scenario enables quantification of the contribution of carbon-concentration and carbon-climate feedback to the changes in carbon fluxes before and after the peaks of CO_2 concentration and temperature. The framework has not been used for overshoot scenarios with the exception of Schwinger & Tjiputra (2018) for the ocean. It is important to understand the carbon-concentration and carbon-climate feedbacks of both land and ocean under overshoot scenarios through this feedback framework. The potential reversibility of feedbacks may influence mitigation pathways to achieve the Paris Agreement goals.

In this study, we take advantage of the newly available results from the state-of-art Earth system models (ESMs) developed under the Coupled Model Intercomparison Project 6, CMIP6 (Eyring et al., 2016) simulated under the shared socioeconomic pathway overshooting scenario named SSP5-3.4-OS (O'Neill et al., 2014). First, we evaluate carbon fluxes by ESMs against observational data sets. This step is required because inaccuracies in estimating past carbon uptakes by land and ocean may propagate to future predictions. Next, we investigate the

spatiotemporal changes in carbon fluxes by six CMIP6 ESMs. Because the SSP5-3.4-OS includes the implementation of bioenergy crops in the future, we attempt to separate the net land flux into land-use emissions from the expansion of bioenergy crops and sinks or sources in other ecosystems. Finally, we apply the carbon cycle feedback framework to quantify the carbon cycle feedbacks of the CMIP6 ESMs under the SSP5-3.4-OS pathway.

2 Description of the overshoot scenario and Earth system models

2.1 SSP5-3.4-OS

The SSP5-3.4-OS experiment is part of the Scenario Model Intercomparison Project, ScenarioMIP (O'Neill et al., 2017; Tebaldi et al., 2020). It is designed to explore the biogeophysical feedbacks of the Earth system to a strong ramp-down phase of CO_2 concentration and temperature after the historical and future steady increase until the mid-century (Meinshausen et al., 2020). The GHG forcing of the SSP5-3.4-OS is based on the REMIND-MAgPIE SSP5 baseline scenario. It was developed by emission-driven simple model MAGICC7.0 and initially follows the high emission (fossil-fuel development) SSP5-8.5 scenario until the 2030s with a steep reduction in CO_2 emissions thereafter due to aggressive mitigation. CO_2 emissions become net zero by 2070s, then go negative up to about -8 GtC year^{-1} by the year 2100, and ramp back to zero by the year 2170 (Figure S1). The total radiative forcing in SSP5-3.4-OS reaches 3.4 Wm^{-2} in 2100. The negative emissions in this overshoot pathway reach a cumulative amount of ca. 230 GtC (starting from the year 2011) by the end of the 21st century (Figure S1) and are achieved by a second-generation bioenergy cropland expansion coupled with carbon capture and storage (CCS), mainly at the cost of pastures (Hurtt et al., 2020).

The SSP5-3.4-OS is a "Tier 2" SSP scenario. It branches from the SSP5-8.5 simulation, which itself branches from the year 2014 of the historical experiment. For the analysis, we use these three adjoined experiments— historical from 1850 to 2014, SSP5-8.5 for the period of 2015–2039, and SSP5-3.4-OS for the period of 2040–2100 (2300). In addition to fully coupled simulations (COU), we use biogeochemically (BGC) coupled simulations of ESMs under the SSP5-3.4-OS pathway to study the carbon cycle feedbacks. The SSP5-3.4-OS-BGC is part of the Coupled Climate–Carbon Cycle Model Intercomparison Project, C4MIP (Jones et al., 2016b). The data are analyzed relative to the preindustrial control (piControl) simulation. As the CO_2 atmospheric concentration is not always reported in the model output, we use directly the input4MIP data set which includes the atmospheric CO_2 concentration pathway used in the concentration-driven simulations (Meinshausen et al., 2016; 2020).

2.2 Earth system models

To date, six CMIP6 ESMs have provided carbon cycle outputs for the SSP5-3.4-OS pathway (Table 1). The models are described in detail elsewhere (Arora et al., 2020; Séférian et al., 2020). Three ESMs, IPSL-CM6A-LR, CanESM5, and CESM2-WACCM, provide extended outputs up to the end of the 23rd century. Five ESMs (apart from CESM2-WACCM) provide outputs for both COU and BGC simulations till the end of the 21st century, and the IPSL-CM6A-LR – till the 23rd century. The presence of both COU and BGC simulation outputs enables investigating the carbon cycle feedbacks parameters under the SSP5-3.4-OS scenario. The six models differ in terms of the structure and the representation of carbon cycle processes. Among them, three models represent explicitly the nitrogen cycle over land, two include a fire component, one has dynamic vegetation, and one accounts for permafrost (Table 1). All models

simulate inorganic carbon in the ocean, and among them, two models also consider dissolved organic carbon.

For the estimates of the land-use change (LUC) emissions, we use a variable *fLUC* that is present in four models (absent in CanESM5 and MIROC-ES2L). For the analysis, we use the carbon fluxes anomalies relative to the branching year values for changes in carbon pools and long-term mean piControl values for changes in carbon fluxes. For both pools and fluxes, we subtract the long-term piControl linear trend to remove any residual trend (Figure S2). In the case of fluxes, we subtract long-term piControl mean values and not the values of branching years to avoid creating a drift caused by the interannual variability. Only one ensemble member was available for all the experiments required. Therefore, for the analysis, we use only one ensemble member of each model documented in Table S1.

171 **Table 1.** Major characteristics of the Earth system models, and their simulation setup considered in our study

ESM	**IPSL-CM6A-LR**	**CNRM-ESM2-1**	**CanESM5**	**UKESM1-0-LL**	**MIROC-ES2L**	**CESM2-WACCM**
Center (country)	IPSL (France)	CNRM-CERFACS (France)	CCCma (Canada)	MOHK (UK)	JAMSTEC/NIES/AORI (Japan)	NCAR (USA)
Reference	(Boucher et al., 2020)	(Séférian et al., 2019)	(Swart et al., 2019a)	(Sellar et al., 2019)	(Hajima et al., 2020)	(Danabasoglu et al., 2020)
SSP5-3.4-OS period	2040-2300	2015-2100	2040-2300	2040-2100	2015-2100	2040-2299
Land carbon	ORCHIDEE, br.2.0	ISBA-CTRIP	CLASS-CTEM	JULES-ES-1.0	VISIT-e	CLM5
Nitrogen cycle	No	Implicit	No	Yes	Yes	Yes
Permafrost	No	No	No	No	No	Yes
Fires	No	Yes (natural)	No	No	No	Yes
Dynamic vegetation	No	No	dynamic wetlands	Yes	No	No
PFT	15	16	4 (CLASS), 9 (STEM)	9 natural and 4 crop/pasture	13	22
LUC	Yes	Yes	Yes	Yes	Yes	Yes
Ocean carbon	PISCES-v2	PISCESv2-gas	CMOC	MEDUSA-2.1	OECO2	MARBL-BEC
Representation of marine sediments*	Meta-model	Meta-model	No	Sediment Box	Meta-model	No
SSP-5-3.4-OS-BGC	Yes (extended till 2300)	Yes	Yes	Yes	Yes	No
esm-SSP5-3.4-OS**	No	No	No	Yes	Yes	No
Data set DOIs***	https://doi.org/10.22033/ESGF/CMIP6.5251	https://doi.org/10.22033/ESGF/CMIP6.4165	https://doi.org/10.22033/ESGF/CMIP6.3673	https://doi.org/10.22033/ESGF/CMIP6.6298	https://doi.org/10.22033/ESGF/CMIP6.5710	https://doi.org/10.22033/ESGF/CMIP6.10094
	https://doi.org/10.22033/ESGF/CMIP6.5195	https://doi.org/10.22033/ESGF/CMIP6.4068	https://doi.org/10.22033/ESGF/CMIP6.3610	https://doi.org/10.22033/ESGF/CMIP6.6113	https://doi.org/10.22033/ESGF/CMIP6.5602	https://doi.org/10.22033/ESGF/CMIP6.10071

	https://doi.org/10.22033/ESGF/CMIP6.5271 https://doi.org/10.22033/ESGF/CMIP6.5269	https://doi.org/10.22033/ESGF/CMIP6.4221 https://doi.org/10.22033/ESGF/CMIP6.4047 https://doi.org/10.22033/ESGF/CMIP6.4223	https://doi.org/10.22033/ESGF/CMIP6.3696 https://doi.org/10.22033/ESGF/CMIP6.3694 https://doi.org/10.22033/ESGF/CMIP6.3600 https://doi.org/10.22033/ESGF/CMIP6.3697 https://doi.org/10.22033/ESGF/CMIP6.3695	https://doi.org/10.22033/ESGF/CMIP6.6405 https://doi.org/10.22033/ESGF/CMIP6.6397 https://doi.org/10.22033/ESGF/CMIP6.6055 https://doi.org/10.22033/ESGF/CMIP6.6409 https://doi.org/10.22033/ESGF/CMIP6.6401 https://doi.org/10.22033/ESGF/CMIP6.5953 https://doi.org/10.22033/ESGF/CMIP6.5929 https://doi.org/10.22033/ESGF/CMIP6.5969 https://doi.org/10.22033/ESGF/CMIP6.12203	https://doi.org/10.22033/ESGF/CMIP6.5767 https://doi.org/10.22033/ESGF/CMIP6.5582 https://doi.org/10.22033/ESGF/CMIP6.5769 https://doi.org/10.22033/ESGF/CMIP6.5512 https://doi.org/10.22033/ESGF/CMIP6.5496 https://doi.org/10.22033/ESGF/CMIP6.5525	https://doi.org/10.22033/ESGF/CMIP6.10115 https://doi.org/10.22033/ESGF/CMIP6.10114

172 * from Séférian et al. (2020)

173 ** esm-SSP5-3.4-OS refers to emission-driven simulation, as opposed to concentration-driven SSP5-3.4-OS and SSP-5-3.4-OS – BGC simulations.

174 ***DOIs refer to the data available through the Earth System Grid Federation. The citations are included in the bibliography.

3 Evaluation of Earth system models

The historical carbon uptake by land and ocean is relatively well constrained, and the land uptake should be nearly zero when cumulated over the last 200 years (Gruber et al., 2019; Khatiwala et al., 2009). Thus, ESMs that simulate too large a land uptake in the historical period should be treated carefully for future predictions. In this section, we evaluate the ensemble of ESMs that we use in a consistent way against corresponding observational data for understanding inter-model discrepancies.

3.1 Data and methods

We evaluate the land and ocean carbon fluxes using three different approaches. First, we compare the decadal means, interannual variability (IAV), and linear trends in global land and ocean carbon uptakes by ESMs with Global Carbon Budget 2019, GCB2019 v.1.0 (Friedlingstein et al., 2019) in 1985–2018. Here we adopt the GCB2019 net land flux computed as a residual between fossil fuel emissions, atmospheric growth, and the ocean uptake rather than the more uncertain land uptake directly estimated by biogeochemical process models. For evaluation of the ocean uptake, we use both values averaged from models and data-driven products.

Second, we evaluate carbon fluxes in nine regions, covering nearly the entire globe, in six ESMs against the estimates, based on the observations of the REgional Carbon Cycle Assessment and Processes (RECCAP) project further harmonized and completed by additional data and synthesized for 9 land regions covering nearly the entire globe (Ciais et al., 2020), the most comprehensive global bottom-up carbon flux synthesis to date.

196 Finally, the two inversion-based data sets, CarbonTracker 2019 (CT2019) by Jacobson et
197 al. (2020) and Copernicus Atmospheric Monitoring Service (CAMS) by Chevallier (2013) are
198 used to evaluate the spatial variation of the land and ocean carbon uptake in 2000–2014.

199 3.2 Results of the evaluation

200 Figure 1 shows the evaluation results of the land and ocean carbon fluxes by ESMs
201 against existing data sets. Note that the observational products of the ocean were corrected to
202 deduce the anthropogenic ocean CO_2 uptake, by removing from their total CO_2 flux estimate a
203 pre-industrial steady-state natural ocean CO_2 outgassing (of about 0.78 GtC $year^{-1}$ from
204 GCB2019). This allows a comparison with the ESMs estimates of anthropogenic ocean uptake
205 relative to their respective piControl (Friedlingstein et al., 2019). The ESMs we considered
206 estimate a higher decadal mean of net land carbon uptake than GCB2019 and slightly
207 underestimate the global mean and IAV of ocean carbon uptake relative to data-driven products
208 (Figure 1a). Among six ESMs, CNRM-ESM2-1 estimates the highest cumulative land carbon
209 uptake and the least cumulative ocean carbon uptake for the historical period of 1850-2014
210 (Figure S3).

211 The ESMs agree with the inversions on the ocean acting as a carbon sink globally.
212 Discrepancies are in the tropical areas of the eastern equatorial Pacific Ocean, the northern
213 Indian Ocean, and along the Californian Current. CNRM-ESM2-1 estimates a lower carbon
214 uptake in the North Atlantic Ocean, and MIROC-ES2L estimates weaker outgassing in the
215 equatorial Pacific Ocean than inversions (Figure 1b). These discrepancies were reported by
216 earlier publications (Hajima et al., 2020; Séférian et al., 2019).

The inter-model spread for the net land carbon uptake is much larger than for the ocean sink. GCB2019 reports a smaller net land carbon sink (including LUC emissions) on average during 1985–2018 than ESMs (Figure 1a). The higher land sink by CNRM-ESM2-1 and MIROC-ES2L in the historical period than GCB2019 and other ESMs corresponds to a larger increase in the land carbon pools (Figure S3). IPSL-CM6A-LR is the closest to GCB2019 in terms of the IAV of the land sink (defined via standard deviation) among the ESMs. MIROC-ES2L and UKESM1-0-LL overestimate IAV, CNRM-ESM2-1 and CESM2-WACCM underestimate it compared to GCB2019. The spatial variations of the net land carbon uptake by the two atmospheric inversions agree in sign but disagree in magnitude with each other, even at the scale of coarse latitude bands (Friedlingstein et al., 2019 and Figure 1b). The inversions estimate a higher land sink in the north than ESMs and a carbon source in the tropics that is not present in the ESMs. MIROC-ES2L estimates slightly higher net biome production (NBP) sink in Northern Hemisphere than other models (that is still lower than in the inversions). UKESM1-0-LL estimates slightly high carbon uptake in the tropical Amazonia and Africa, which Sellar et al. (2019) attributed to a small overestimation of tree fraction in savanna biomes compared to observational data sets.

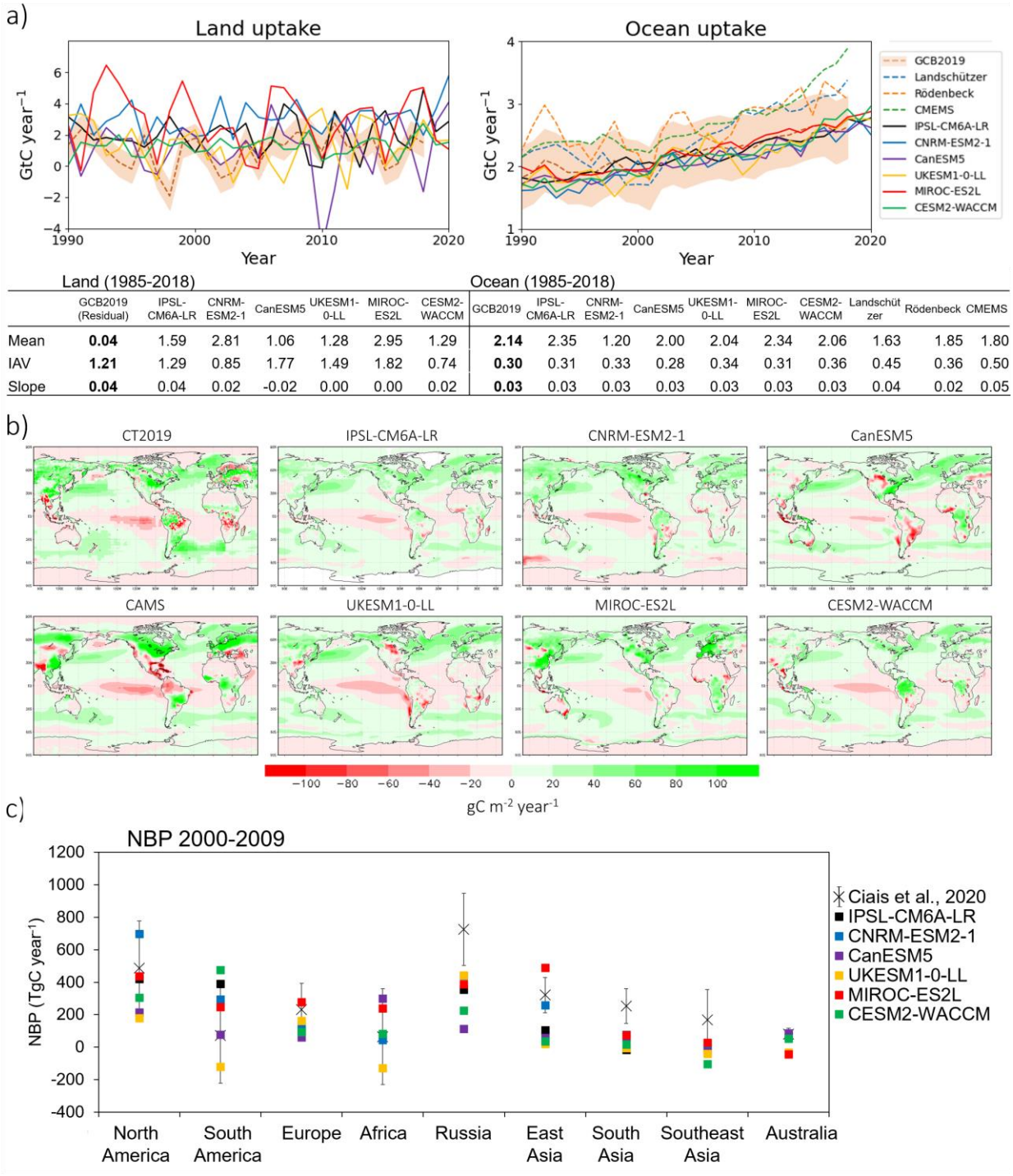

Land (1985-2018)

	GCB2019 (Residual)	IPSL-CM6A-LR	CNRM-ESM2-1	CanESM5	UKESM1-0-LL	MIROC-ES2L	CESM2-WACCM
Mean	**0.04**	1.59	2.81	1.06	1.28	2.95	1.29
IAV	**1.21**	1.29	0.85	1.77	1.49	1.82	0.74
Slope	**0.04**	0.04	0.02	-0.02	0.00	0.00	0.02

Ocean (1985-2018)

	GCB2019	IPSL-CM6A-LR	CNRM-ESM2-1	CanESM5	UKESM1-0-LL	MIROC-ES2L	CESM2-WACCM	Landschützer	Rödenbeck	CMEMS
Mean	**2.14**	2.35	1.20	2.00	2.04	2.34	2.06	1.63	1.85	1.80
IAV	**0.30**	0.31	0.33	0.28	0.34	0.31	0.36	0.45	0.36	0.50
Slope	**0.03**	0.03	0.03	0.03	0.03	0.03	0.03	0.04	0.02	0.05

Figure 1. An evaluation of Earth system models (ESMs) against observational and inversion datasets. The sign convention is that sources of CO_2 to the atmosphere are negative values and removals/sinks are positive. Panel (a) shows the interannual variability of land (net biome

237 production, NBP) and ocean (fgco2) carbon uptakes by ESMs and Global Carbon Budget
238 (GCB2019) and three data-driven products (Denvil-Sommer et al., 2019; Landschützer et al.,
239 2016; Rödenbeck et al., 2014). Data-driven products are corrected for pre-industrial outgassing
240 of 0.78 GtC $year^{-1}$. Shaded area indicates uncertainty provided by Friedlingstein et al. (2019).
241 The residual NBP values for GCB2019 in the table are calculated using the GCB2019 ocean
242 uptake that is the average of several global ocean biogeochemistry models that reproduce the
243 observed mean ocean sink of the 1990s. Panel (b) shows the 2000–2014 mean annual carbon
244 uptake by land and ocean estimated by ESMs and two atmospheric inversions CT2019 and
245 CAMS. Panel (c) shows NBP for nine RECCAP regions in 2000–2009 according to Ciais et al.
246 (2020). Error bars indicate estimates of uncertainty from Ciais et al. (2020).

247 All ESMs estimate lower land carbon uptake in Russia, South Asia, and Southeast Asia
248 than the corresponding inventory-based estimates in RECCAP (Figure 1c). To understand the
249 reasons for this underestimation, we compared other land fluxes by ESMs with those given by
250 Ciais et al. (2020) (Figure S4). ESMs adequately estimate net primary production (NPP) relative
251 to RECCAP. CESM2-WACCM and IPSL-CM6A-LR reproduce heterotrophic respiration (R_H)
252 well. However, most models estimate higher than RECCAP estimates R_H in North America, East
253 Asia, South-East Asia, and Australia, possibly because they do not include harvest processes that
254 decouple NPP from R_H. The *fLUC* emissions are underestimated by ESMs in tropical regions.
255 This likely reflects the fact that *fLUC* diagnosed by ESMs follows a definition that does not
256 cover all LUC emission terms of the models' realm (e.g., legacy soil carbon emissions after
257 LUC, biomass decay after LUC are not in *fLUC*). There is also the fact that models do not
258 reproduce some LUC emission processes such as shifting cultivation or degradation that were
259 included in the LUC emissions from RECCAP. The difference between NPP and R_H is higher in

RECCAP estimates than in ESMs in all regions. Thus, these component fluxes cannot explain the discrepancies between ESM and RECCAP estimates, suggesting there could still be missing processes in these state-of-the-art models (Ciais et al., 2020).

4 Analysis of the carbon cycle feedbacks under the SSP5-3.4-OS pathway

4.1 Temporal variation of global carbon fluxes under SSP5-3.4-OS

In the concentration-driven SSP5-3.4-OS scenario, the CO_2 concentration as given by input4MIPs peaks in the year 2062 at 576.2 ppm (Figure 2). According to the scenario design, strong mitigation policies to reduce GHGs emissions, which include bioenergy crops and CCS expansion, start in 2040 and result in an immediate decrease in the CO_2 growth rate that peaks in 2041 (O'Neill et al., 2017; Meinshausen et al., 2020). Both peaks of the CO_2 concentration and CO_2 growth rate have important implications on the carbon fluxes discussed hereafter.

The six ESMs demonstrate large differences in the response of global mean surface air temperature (GSAT) to the prescribed changes in CO_2 concentration under the SSP5-3.4-OS. The magnitudes of the overshoot vary from 2.4 °C in MIROC-ES2L to 4.1 °C in CanESM5, the timings of the GSAT peaks vary from the late 2040s in MIROC-ES2L to the late 2070s in CNRM-ESM2-1, and the rates of the GSAT ramp-down vary from a steep decrease in CanESM5 to almost no decrease in CNRM-ESM2-1. In all six ESMs, the growth rate of GSAT peaks in the early 2040s, just a few years after the peak of the CO_2 growth rate (Figure S5).

The land and ocean carbon uptake always decrease after the peak of the CO_2 growth rate (and before the peak of CO_2 concentration). However, these two reservoirs continue to remove CO_2 from the atmosphere at least for 50 years (Figures 2b and 2c). Three models, IPSL-CM6A-LR, CanESM5, and CESM2-WACCM, which provide COU simulation outputs for the 22nd and

23rd-century extension, show that the land and ocean turn into a carbon source for a limited time in the 22nd century. CanESM5 simulates a larger temperature overshoot than IPSL-CM6A-LR and CESM2-WACCM and corresponding longer periods of land and ocean acting as carbon sources in the first half of the 22nd century. At the end of the 22nd century, the land becomes nearly net-zero and the ocean remains a weak carbon sink. Among three ESMs, CESM2-WACCM –that accounts for permafrost processes– has the lowest value of land carbon uptake (zero to weak source) at the end of the 23rd century. It simulates a continued carbon source from high latitude carbon soils till the end of the study period that is almost entirely compensated by the vegetation greening (Figure S6). By the end of the 23rd century, all models agree that the accumulated carbon is stored mainly in the Southern Ocean and over mid-to-high latitudes of the Northern Hemisphere in the land. When looking at the changes in the carbon reservoirs (Figure S3c), the ESMs agree that during the ramp-down, the ocean releases some previously stored carbon to the atmosphere for a limited period (of around 50 years) and continues to take up carbon at a decreased rate thereafter. The long-term response of land to the overshoot largely differs among ESMs to the extent from returning to the preindustrial levels of carbon storage in CanESM5 to the increase in land carbon pool half the size of the ocean pool in IPSL-CM6A-LR.

The estimated behavior of land and ocean under overshoot is consistent with existing studies. Jones et al. (2016) used four ESMs and RCP2.6 scenario, which has an earlier peak of CO_2 growth rate (and CO_2 concentration) and a slower ramp-down phase than this study. They reported that land and ocean remain carbon sinks for more than 100 years after the peak of the CO_2 growth rate. Palter et al. (2018) used one ESM and RCP8.5-based overshoot scenario, which has a later peak of CO_2 growth rate (and CO_2 concentration) and a more rapid ramp-down phase than this study. They reported that land and ocean turn to carbon sources in less than three

decades after the peak of CO_2 concentration. Based on the three studies, earlier CO_2 peak and slower ramp-down cause the land and ocean to act as carbon sinks for a longer time.

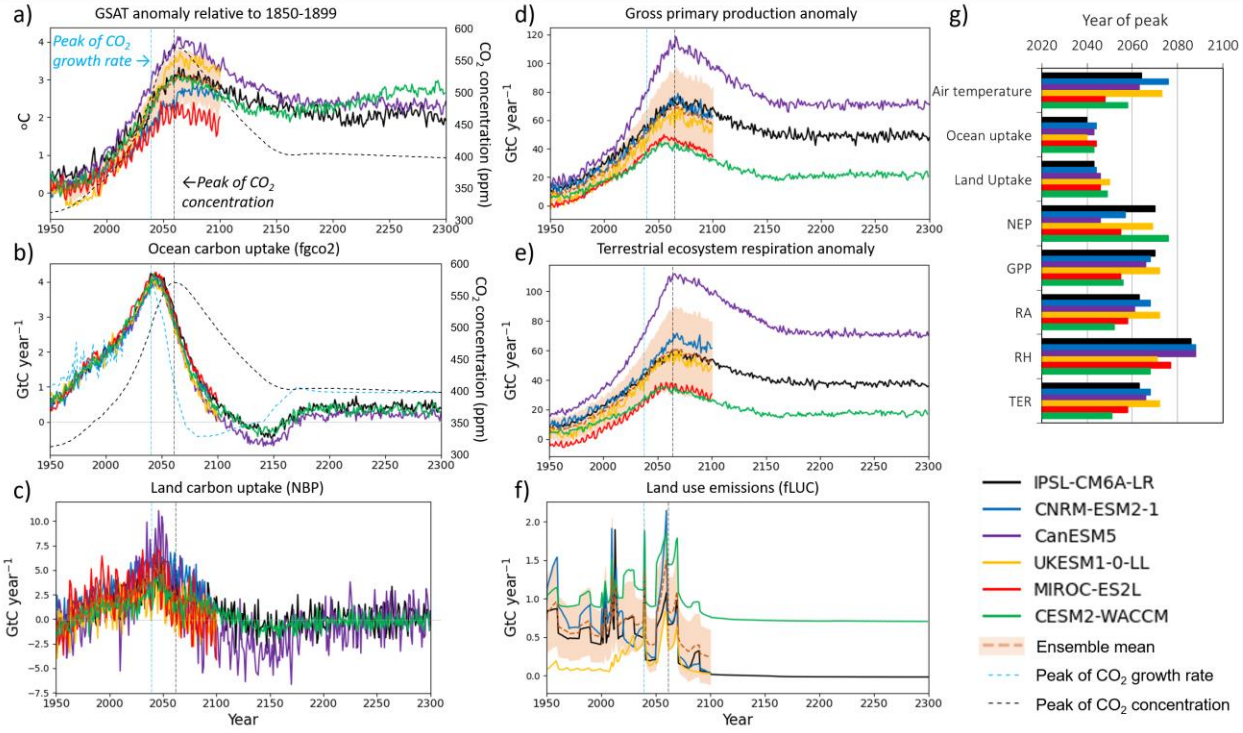

Figure 2. Time series and peak years of the global annual total or mean variables of ESMs, including (a) GSAT, and CO_2 concentration, (b) ocean uptake, (c) NBP, (d) GPP, (e) TER, and (f) LUC emissions. Air temperature anomaly is taken from 1850–1899 mean; other variables are anomalies from piControl simulation. The ensemble mean (dashed brown line) of six ESMs is calculated till the year 2100 with a shaded area indicating ensemble spread via standard deviation. The CO_2 concentration and its growth rate are shown with dashed black and blue curves on panels (a) and (b). The years of peak atmospheric CO_2 concentration and CO_2 growth

rate are indicated by vertical black and blue dashed lines, respectively. The panel (g) indicates the years of peak of the variables.

4.2 The peaks of land and ocean carbon uptakes

The peaks of carbon uptake by land and ocean occur before the peaks of CO_2 concentration, temperature, gross primary production (GPP), terrestrial ecosystem respiration (TER), and its components autotrophic (R_A) and heterotrophic (R_H) respirations (of which R_H peaks the latest). To identify the reasons for those varying peak times, it is essential to look at the derivatives of the variables (Figures S7).

The response of air temperature lags CO_2 concentration, owing to the inertia of the climate system at the time the CO_2 starts to decrease. McKinley et al. (2020) and Schwinger and Tjiputra (2018) pointed out that the CO_2 growth rate dominates the variability in the global ocean on year-to-year timescales, hypothesizing that other internal and external drivers may become more important in the altered state of the ocean in the future. Based on the outputs of six CMIP6 ESMs, we show that global ocean carbon uptake is nearly a linear function of the atmospheric CO_2 growth rate, confirming the finding discussed above. The slope of the function changes after the peak of the CO_2 growth rate from 0.74 ± 0.03 to 0.26 ± 0.02 GtC year^{-2} (average and standard deviation of six ESMs), with a clear hysteresis behavior (Figure 3b). At the peak of the CO_2 growth rate, the linear function curls up with the negative CO_2 growth values. The extended simulation outputs available for three models indicate that the trajectory of the ocean uptake curve is directed towards zero, closing the cycle after a limited period of carbon source. Understanding the mechanism of this strong dependency requires additional analysis and should

be confirmed on the different overshoot scenarios

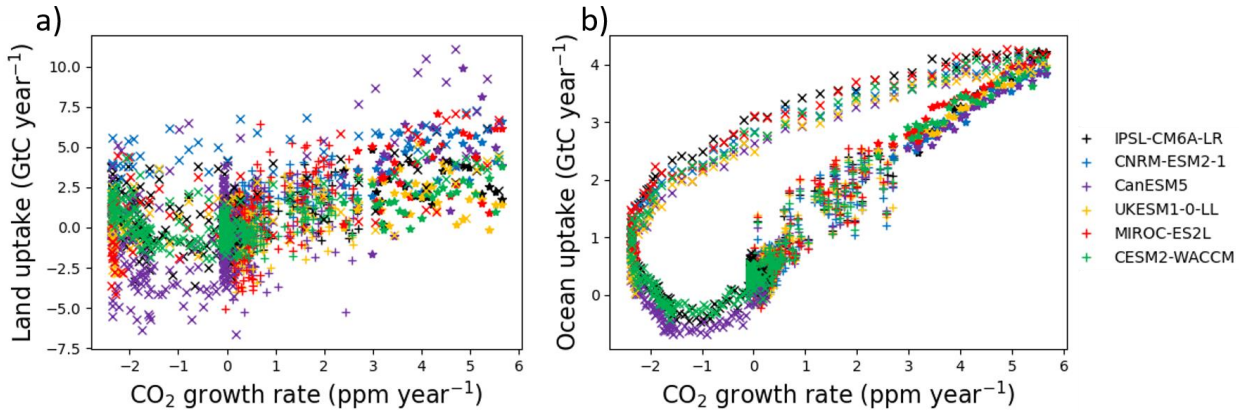

Figure 3. The dependency of (a) land and (b) ocean carbon uptake on the atmospheric CO_2 growth rate by CMIP6 Earth system models under historical and SSP-5-3.4-OS pathway. The markers "+" indicate the historical period (1850–2014), markers "*" and "×" indicate the periods before and after the peak of CO_2 growth rate in 2041, respectively.

The ESMs reveal a weaker linear dependency of the land carbon uptake on the CO_2 growth rate than on the ocean uptake (Figure 3a). It is well-known that the two largest land carbon fluxes, namely GPP and TER, primarily depend on the CO_2 concentration, temperature, and soil moisture, as well as other factors not modeled by ESM such as land management intensity, and nutrient limitations (Ciais et al., 2020; Huntzinger et al., 2017). Furthermore, R_H depends on the soil carbon pools and their turnovers which themselves are a lagged function of NPP. This dependency leads to a lagged response of the TER, and particularly R_H, growth rates compared to that of GPP, which is well recognizable in MIROC-ES2L and UKESM1-0-LL (Figures 2 and S7a).

4.3 Impact of land-use change emissions

The changes in the growth rate of GPP and TER alone cannot explain the early land carbon uptake peak in some models such as IPSL-CM6A-LR. The anthropogenic LUC emissions due to the expansion of the bioenergy crops in the 2040s may also contribute to the early peak of the land carbon uptake although models do not represent explicitly the higher yield or specific biophysical parameters if bioenergy crops (to our knowledge). The only type of anthropogenic carbon emissions that increases after the 2040s of the SSP5-3.4-OS is those of agriculture, forestry, and other land use (AFOLU, Figure S8). We postulate that both the larger growth rate of TER than GPP and increased LUC emissions cause the early peak of land uptake. The expansion of biofuel crops may cause a weakening of the land sink capacity because these systems dedicated to biomass production for harvest no longer have the potential for storing carbon e.g., in soils or biomass.

The spatial variation of the bioenergy cropland area expansion under the SSP5-3.4-OS is formulated in the Harmonization of Global Land-Use Change and Management (LUH2) data set (Hurtt et al., 2020). In most ESMs, the areas where the bioenergy crops are implemented correspond to areas of decreases in the land carbon uptake after the CO_2 growth rate peaks compared to the prior period, e.g., eastern South America, Europe, the eastern coast of North America, and the northern part of Southeast Asia (Figures S7b, S9, and S10). A strong impact of LUC on the carbon uptake is remarkable for the IPSL-CM6A-LR and UKESM1-0-LL. Yet, the effect of LUC on newly converted bioenergy croplands vs. those of climate change on remaining natural ecosystems cannot be separated in each ESM grid cell, from the available simulations. The modeling groups use varying definitions of the land-use change due to different system boundaries and different definitions of the human perturbation of ecosystems resulting in

inconsistent reporting of LUC emissions estimates among the ESMs (Gasser & Ciais, 2013). This uncertainty should be addressed in related future intercomparison projects.

5 Quantifying the Carbon cycle feedbacks under the SSP5-3.4-OS pathway

5.1 Definitions and method

We apply the carbon cycle feedback framework on the five ESMs (apart from CESM2-WACCM) that have all the necessary data for calculations explained below. The carbon-concentration feedback parameter (β, GtC ppm^{-1}) indicates the changes in the carbon storages of land and ocean in response to changes in the atmospheric CO_2 concentration. The carbon-climate feedback parameter (γ, GtC $°C^{-1}$) indicates the changes in the carbon storage in response to the changes in GSAT. The change in the carbon storages of land and ocean can then be decomposed into the β and γ contributions ($\beta \times \Delta CO_2$ and $\gamma \times \Delta T$, respectively), and a residual term ε:

$$\Delta C = \beta \times \Delta CO_2 + \gamma \times \Delta T + \varepsilon \quad (1)$$

The β contribution (or β uptake) is the changes in carbon storage (GtC) or flux (GtC $year^{-1}$) credited to the carbon-concentration feedback and γ contribution is the changes in carbon storage or flux credited to the carbon-climate feedback. ΔC is the difference in the carbon storage relative to the piControl simulation, ΔCO_2 is the difference in the global atmospheric CO_2 concentration relative to the value of the year 1850 as given by input4MIP (284.32 ppm), and ΔT is the difference in temperature simulated by each ESM relative to 1850–1899 mean GSAT. In the case of the SSP5-3.4-OS, neither ΔCO_2 nor ΔT become negative any time after the peaks.

The carbon cycle feedback parameters can be diagnosed from the differences in COU, BGC, and radiatively coupled (RAD) simulations of ESMs. In the BGC simulation, only changes in the CO_2 concentration, and not temperature, affect the land and ocean carbon-cycle processes.

In the RAD simulation, in contrast, changes in the CO_2 concentration affect the radiation balance of the atmosphere but are not seen by the carbon cycle. There are two commonly used approaches to estimate the carbon cycle feedback parameters, (1) β from BGC, γ from RAD, and (2) β from BGC, γ from the difference between COU and BGC (thereafter, COU–BGC). In this study, we used the latter approach because no RAD simulations are currently available for SSP5-3.4-OS. In this case, the residual term ε of Equation (1) is integrated into γ. Previous studies show that the absolute values of γ estimated by the COU–BGC approach can appear 2–3 times larger than the RAD approach because RAD simulation does not include the suppression of carbon transport to the deep ocean due to weakening ocean circulation (Schwinger & Tjiputra, 2018; Arora et al., 2020).

We estimate β and γ for land (β_{land} and γ_{land}) and ocean (β_{ocean} and γ_{ocean}) using the land carbon pool (*cLand*) and cumulative ocean carbon flux (*fgco2*) because not all models provide the ocean carbon pools (*dissic* and *dissoc*). Before calculations, we confirmed that β and γ estimated using the carbon pool variables agree with corresponding estimates obtained from the cumulative carbon fluxes, i.e., *NBP* and *cLand* over land and *fgco2* and *dissic+dissoc* over the ocean (not shown). Furthermore, we decomposed the land β in terms of underlying processes, such as GPP, R_A, and R_H, using cumulative fluxes over time.

5.2 Carbon cycle feedbacks before mitigation activities

The β and γ feedback parameters depend on the state of the system and scenario (Friedlingstein et al.; 2006, Jones et al., 2016b; Willeit et al., 2014). To understand the carbon cycle feedbacks under the SSP5-3.4-OS overshoot pathway, it is essential to first investigate the changes in the carbon pools (that define the state of the system) over the historical period. ΔC of the five ESMs varies in the historical period to the extent that ΔC_{land} is either positive, e.g., in

418 CNRM-ESM2-1, IPSL-CM6A-LR, and UKESM1-0-LL, or negative, e.g., in CanESM5 and
419 MIROC-ES2L (Figure S3), resulting in positive and negative β (Figures 4 and 5) at the
420 beginning of the 21st century.

421 Before the peak of CO_2 concentration, β_{ocean} decreases (becomes less positive) in all five
422 ESMs (Figure 4a). We speculate this happens because increasing anthropogenic carbon
423 emissions exceed the ability of the ocean to absorb carbon (Friedlingstein et al., 2019). In all
424 models apart from CNRM-ESM2-1, β_{land} increases at the beginning of the 21st century and
425 continues to increase after the CO_2 concentration peak at a rising rate. CNRM-ESM2-1 exhibits
426 larger uptake during the historical period before the year 2000 that, perhaps, causes high ΔC
427 already at the beginning of the 21st century, leading to overly high β_{land}. Besides, unlike other
428 models, CNRM-ESM2-1 shows decreasing positive γ_{ocean} throughout the study period.

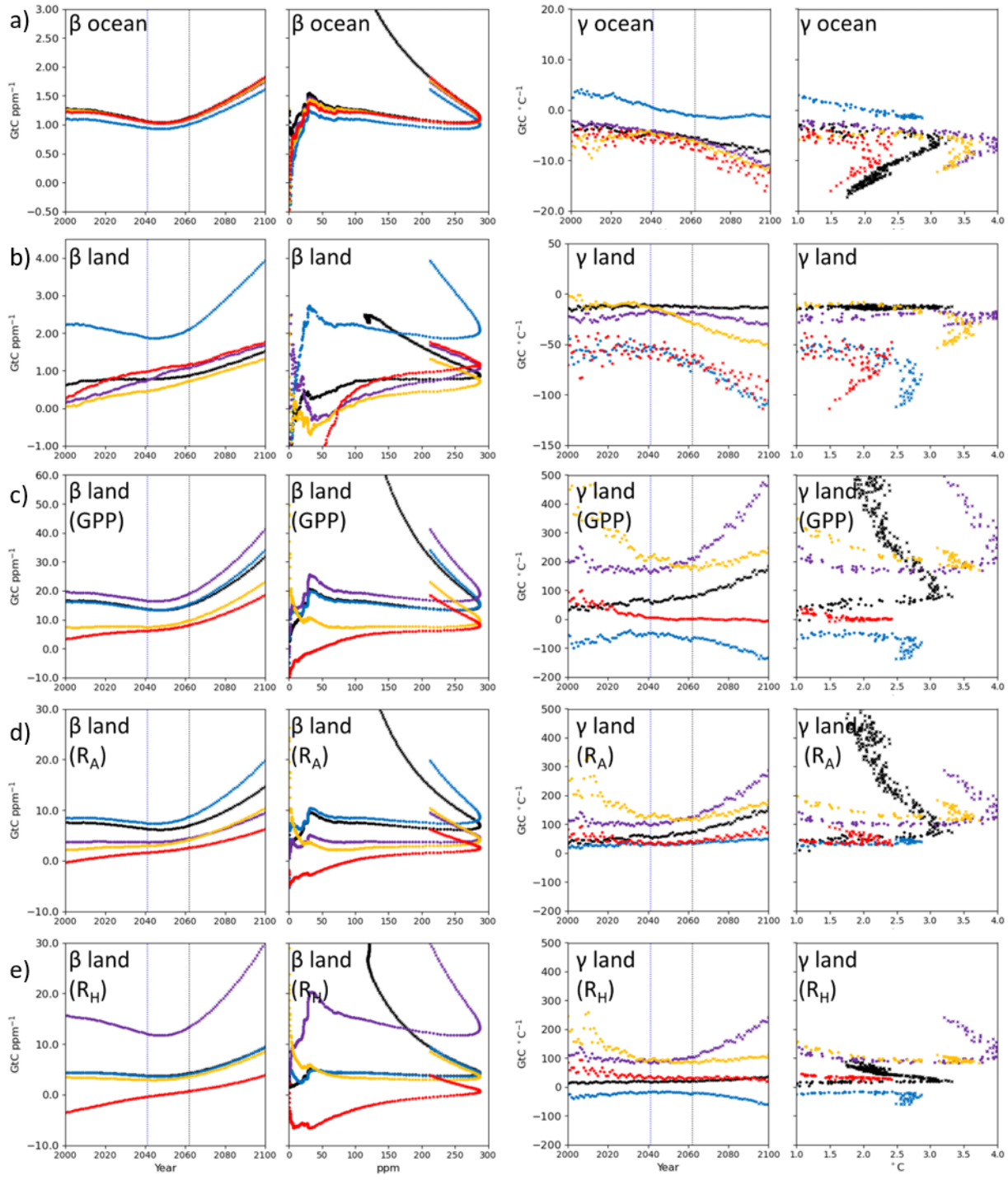

Figure 4. Carbon-concentration β (GtC ppm^{-1}) on the left and carbon-temperature γ (GtC $°C^{-1}$) feedback parameters for (a) ocean estimated from cumulative flux fgco2, and (b) land estimated

from cumulative NBP. Estimated feedback parameters for cumulative land fluxes: (c) GPP, (d) $R_{A,}$ and (e) R_H. The figures in the first column show β as a function of time (year) and in the second column as a function of ΔCO_2 concentration (ppm). The figures in the third column show γ as a function of time (year) and in the fourth column as a function of temperature (°C). GPP, NBP, and fgco2 are positive to the surface, R_A and R_H are positive to the atmosphere. We use data extended to 2300 for IPSL-CM6A-LR. In the first and third columns, the years of peak atmospheric CO_2 concentration and CO_2 growth rate are indicated by vertical black and blue dashed lines, respectively.

5.3 Magnitudes of carbon cycle feedbacks under SSP5-3.4-OS

Apart from CNRM-ESM2-1, the strength of the β feedback parameter by ESMs is similar over land and ocean, the strength of the negative γ parameter is larger over land than over ocean (Figures 4a and 4b). The magnitude of global transient γ_{land} at the maximum exceeds γ_{ocean} nearly 1.5 times in IPSL-CM6A-LR, 2–3 times in CanESM5 and UKESM1-0-LL, and 10–20 times in CNRM-ESM2-1 and MIROC-ES2L. This agrees with a study based on the idealized 1% CO_2 increase 2 × CO_2 and 4 × CO_2 scenarios (see Table A1 of Arora et al., 2020) and persists in both ramp-up and ramp-down stages of overshoot.

The β and γ feedback parameters are calculated as a ratio of carbon pool or cumulative flux (relative to piControl size) per unit change CO_2 concentration and temperature. They increase their absolute values after the peaks of CO_2 and temperature, i.e., β becomes more positive and γ more negative (Figure 4). This happens because, on the one hand, the carbon pool, i.e., the numerator of the ratio, continues to increases after the peaks, and on the other hand, ΔCO_2 or ΔT from pre-industrial values, i.e., the denominator, decreases. Although an additional analysis with the use of a suite of overshoot pathways is necessary to gain further insights, there

455 are several hypotheses. First, the legacy effects, i.e., larger carbon pool gained during the ramp-
456 up period, may cause amplification of causing β and γ feedback parameters over land. The larger
457 the carbon pool is, the more it can gain via β feedback and lose via γ feedback, unless the
458 saturation is reached. Second, the aggressive CO_2 mitigation applied in the SSP5-3.4-OS
459 scenario, where carbon is removed from the atmosphere away to the geological reservoirs,
460 further reduces ΔCO_2 and, thus, contributes to the amplification of the β parameter (Figures 2
461 and S1). The decline in air temperature is delayed after the CO_2 concentration and is not
462 absolutely reversible under the timescales of this study. The amplification of the γ parameter
463 after the air temperature peak occurs in all ESMs apart from IPSL-CM6A-LR (due to
464 compensating effects) and is driven by the hysteresis in the changes in the carbon pools that
465 continue to increase for several decades after the GSAT peaks and by the delayed temperature
466 response.

467 IPSL-CM6A-LR is the only ESM that included both extended to the 23rd century BGC
468 and COU simulations that are necessary for the calculation of β and γ. At the end of the 23rd
469 century, CO_2 concentration is around 398 ppm and air temperature warming relative to pre-
470 industrial value is around 1.9 °C. This ESM, unlike others, estimated nearly constant γ_{land}. The
471 model outputs show a continued amplification of β_{ocean} and γ_{ocean} at a reduced rate after the 2150s
472 and nearly constant β_{land} and γ_{land} after the 2150s (Figure S11). This behavior of β and γ
473 translates into nearly steady states of land and ocean carbon fluxes (Figure 2). By the end of the
474 23rd century, land and ocean storages increase by 180 and 416 GtC relative to the preindustrial
475 levels, respectively.

476 5.4 Spatial variation of transient carbon cycle feedbacks under overshoot

477 The spatiotemporal variation of the changes in β and γ parameters clarifies the inter-
478 model differences (Figure 5). β_{ocean} strengthens during the ramp-down in the mid-latitudes of the
479 Northern Hemisphere and equatorial zone and increases over the Southern Ocean. In many areas
480 of β_{ocean} increase, γ_{ocean} also intensifies, perhaps, due to the increases in the ocean pool.

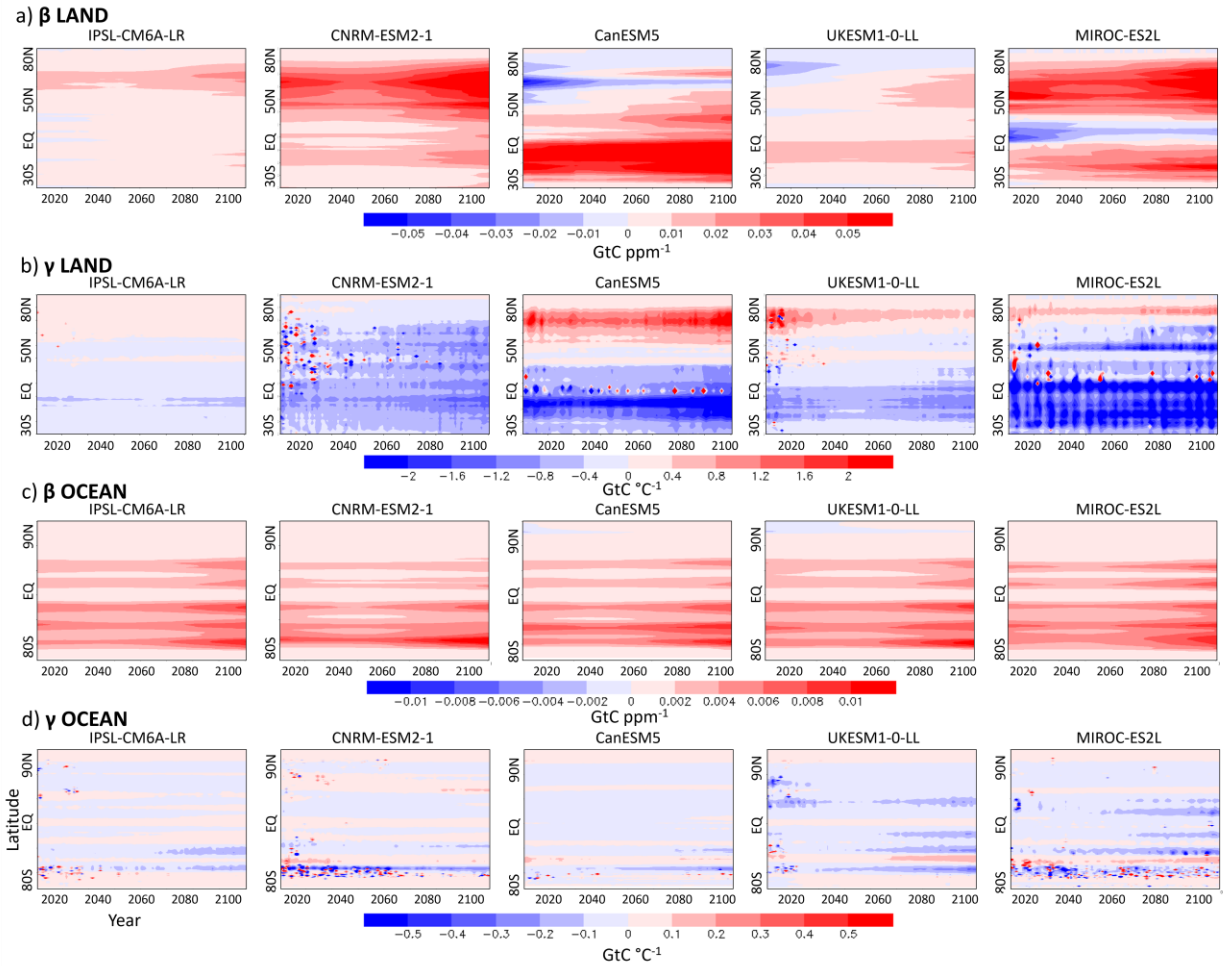

481

482 **Figure 5.** The spatiotemporal variation of zonal cumulative (a) β_{land} (GtC ppm^{-1}), (b) γ_{land} (GtC
483 $°C^{-1}$), (c) β_{ocean} (GtC ppm^{-1}) and (d) γ_{ocean} (GtC $°C^{-1}$) calculated from land carbon pool and
484 cumulative ocean uptake. Positive values indicate a net sink.

The spatial variation of β_{land} and γ_{land} is strikingly diverse among models. ESMs agree that β_{land} is positive in the equatorial region, and it increases during the ramp-up but decreases during the ramp-down. CanESM5and UKESM1-0-LL have negative β_{land} over mid-latitudes till the 2040s that is compensated by the positive γ_{land}. The negative γ_{land} over tropics in MIROC-ES2L is maintained throughout the study period, although it keeps decreasing (Figure 5). The negative β_{land} emerges due to the decrease of ΔC_{land} below the pre-industrial value before ramping back by the end of the 21st century (Figures S3 and S12). The decrease in ΔC_{land} corresponds to the decrease in ΔC_{soil} in CanESM5, and ΔC_{veg} in MIROC-ES2L and UKESM1-0-LL.

The γ_{land} is positive in the high latitudes and negative in the equatorial regions, as estimated by all ESMs except for CNRM-ESM2-1. The distinct changes in CNRM-ESM2-1 in the idealized scenarios were discussed by Arora et al. (2020) and attributed to the larger nonlinearity effects compared to other models. The negative γ_{land} in CNRM-ESM2-1 emerges due to negative γ_{soil}, while γ_{veg} stays positive through the study period (Figure S13). After the peak of air temperature, the positive γ_{land} over high latitudes of the Northern Hemisphere amplifies in CanESM5 and UKESM1-0-LL, stays without a change in IPSL-CM6A-LR, and weakens in MIROC-ES2L. None of the five ESMs includes the permafrost component. Thus, the question –whether the positive γ_{land} over high latitudes continues to increase during the ramp-down phase of temperature overshoot or decreases– remains open. The γ_{land} is increasingly negative in the equatorial zone (probably due to drying, Figure 5b). Overall, our results imply that the amplification of the β_{land} after overshoot is driven by the high latitudes, and the amplification of γ_{land} is driven by the equatorial regions.

5.5 Implication of changes in carbon cycle feedback metrics to the carbon fluxes under overshoot

Due to the dependency of the β uptake on the CO_2 growth, it starts to decrease in the early 2040s, leading to the peaks of the land and ocean uptakes in 2040s concurrent with the peak of CO_2 growth rate (Figures 6a and 6b). The γ uptake peaks later due to temperature change lagging behind the atmospheric CO_2 change. Although the values of β and γ parameters (>0 for β and <0 for γ) increase after the peaks of CO_2 and temperature, opposing each other, the total γ-driven loss of carbon is smaller than β gain at least till the end of the 21st century. The changes in the carbon cycle are dominated by β rather than γ. While existing studies show that during the ramp-up period, the positive contribution of the β is larger than the γ-driven loss (Arora et al., 2020), we demonstrate here for the first time that this remains valid for the ramp-down period under SSP5-3.4-OS based on the five CMIP6 ESMs under consideration.

Apart from CNRM-ESM2-1 that has positive γ_{ocean}, ESMs show that the amplification of β_{ocean} and γ_{ocean} during the ramp-down period cause the ocean to uptake more carbon compared to if β_{ocean} and γ_{ocean} were fixed at the level of the peaks of CO_2 concentration and temperature (Table S2). The feedback amplification leads to a larger β uptake and larger γ loss (Figure S14). All models agree that amplification β_{land} and γ_{land} lead to a larger cumulative land carbon uptake by the year 2100 under the SSP5-3.4-OS pathway.

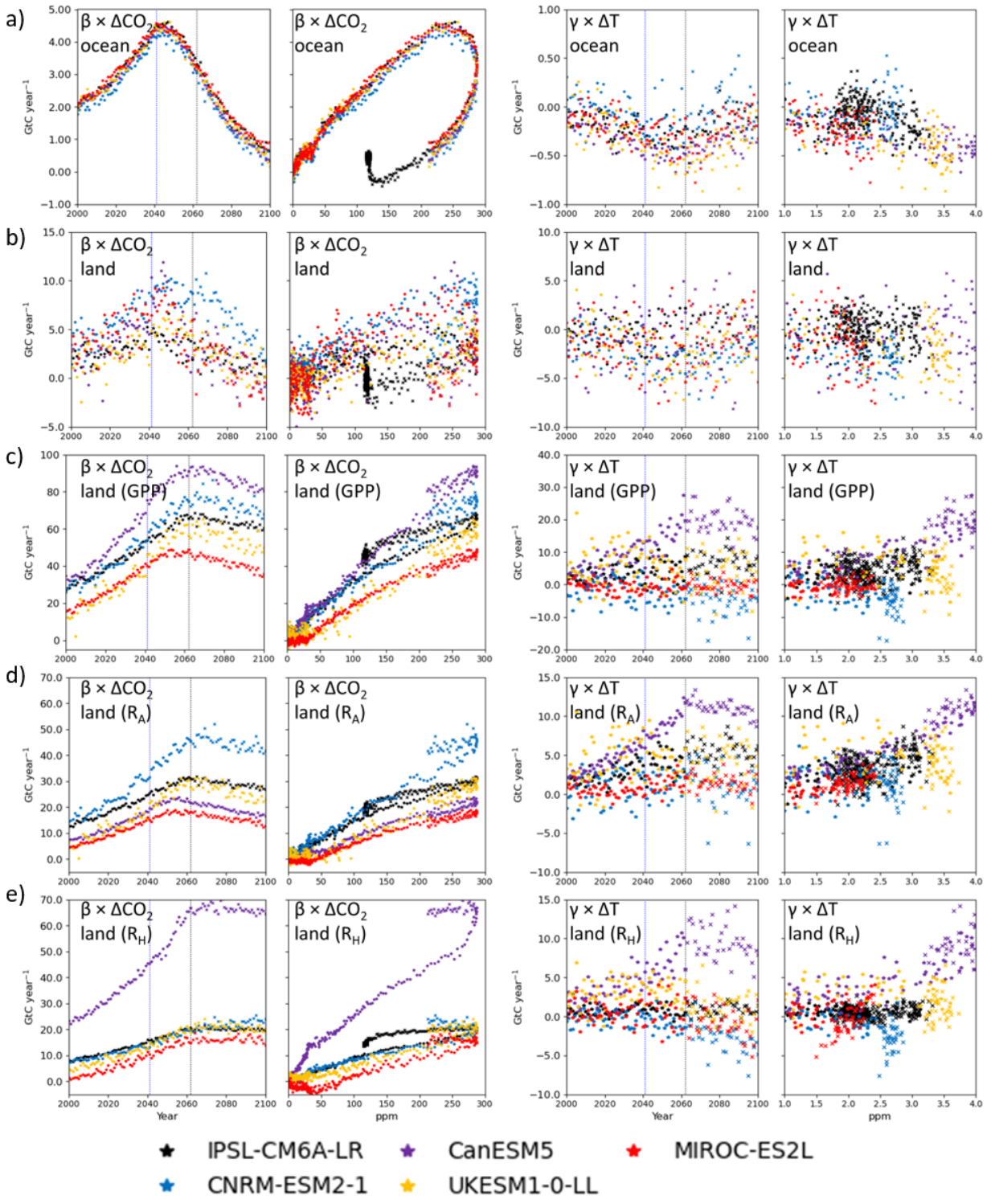

Figure 6. Breakdown of land and ocean carbon uptakes to the contributions of β and γ (GtC year^{-1}) as a function of time, CO_2 concentration, and temperature. Contributions are calculated as

yearly change of $\beta \times \Delta CO_2$ and $\gamma \times \Delta T$ for (a) ocean carbon uptake fgco2, (b) NBP, (c) GPP, (d) R_A and (e) R_H. The figures in the first column show β as a function of time (year) and in the second column as a function of CO_2 concentration (ppm). The figures in the third column show γ as a function of time (year) and in the fourth column as a function of temperature (°C). GPP, NBP, and fgco2 are positive to the surface, R_A and R_H are positive to the atmosphere. We use extended to 2300 data for IPSL-CM6A-LR. . In the first and third columns, the years of peak atmospheric CO_2 concentration and CO_2 growth rate are indicated by vertical black and blue dashed lines, respectively. The markers "*" and "×" indicate the periods before and after the peak of CO_2 concentration in 2062, respectively.

5.6 Decomposition of β_{land} and γ_{land} into the β and γ of their constituent gross fluxes

We further decompose β_{land} and γ_{land} into the β and γ of their constituent gross fluxes, to investigate the processes behavior before and after the peaks of CO_2 and temperature (Figures 4, 6, S15 and S16). β of GPP, R_A, and R_H (β_{GPP}, β_{RA}, and β_{RH}) exhibit similar behavior with a nearly parallel change, albeit with an opposite impact on the land uptake (Figures 4 c–e). All ESMs demonstrate a larger β_{GPP} than β_{RA} and β_{RH} together, which provokes positive β_{land} feedback during the study period. Global values of γ_{GPP}, $\gamma_{RA,}$ and γ_{RH} are positive, except for CNRM-ESM2-1, while they are negative in the equatorial region for most ESMs (Figure S16). This means that warmer temperatures under the SSP5-3.4-OS do not inhibit photosynthetic processes in the warm regions to a level that surpasses the benefits of warming on the global ecosystem.

Unfortunately, most ESMs used in this study did not include permafrost or vegetation fire components. By considering permafrost emissions, which roughly speaking are equivalent to γ becoming more negative, Gasser et al. (2018) estimated that to achieve the 2 °C target of the

Paris Agreement, the remaining emission budget is reduced by 16% for 0.5 °C overshoot and by 25% for 1 °C overshoot. CESM2-WACCM, the only ESM we considered that resolves the permafrost active layer, did not have BGC simulation outputs under the SSP5-3.4-OS pathway at the time of this analysis. While it would be extremely interesting to look at the carbon cycle feedbacks simulated by this model, its land and ocean carbon uptake estimates nearly median temporal variation of the carbon uptakes among our five ESMs (Figure 2). Based on the spatiotemporal variation of soil carbon storage by the model (Figure S6), we speculate that the permafrost fluxes are not significant in this scenario. Although in CESM2-WACCM, after the air temperature peaks in 2058 (Figure 2), the land pool loses soil carbon in the high latitudes, the loss is mainly attributed to medium soil pool with residence time <100 years (not shown), and it is compensated by vegetation greening in the region. Thus, the permafrost fluxes are not significant for the global carbon uptake, likely because the overshoot size under consideration in the present study is not extremely large. Yet, they may become significant for larger magnitudes of temperature overshoot, and it is necessary to explore permafrost feedback under different overshoot pathways.

6 Conclusion

This study investigated the carbon cycle response of the six CMIP6 ESMs to the temperature overshoot under the SSP5-3.4-OS pathway. The land and ocean continue to remove carbon from the atmosphere at least for 50 years after the peak of the CO_2 growth rate. They only turn to a source afterward in the first half of the 22nd century for a short period and become a weak sink later, i.e., reach a new steady-state. From the perspective of the carbon cycle feedback framework, the land and ocean act as a carbon sink during both ramp-up and ramp-down stages

of overshoot in the 21st century because the β carbon gain $\beta \times \Delta CO_2$ is large than γ loss $\gamma \times \Delta T$ under the considered pathway.

The decrease in the land and ocean uptakes occurs immediately after the start of mitigation efforts, and before the peaks of CO_2 concentration and temperature. The decrease in ocean uptake is driven by the dependency of the ocean sink on the CO_2 growth rate. The decrease in land uptake is caused by the net effect of the decreasing rate of GPP increase and the increase in TER due to delayed warming after CO_2 concentration change. Besides, land-use change emissions induced by the broad expansion of biofuel crops in SSP5-3.4-OS contribute to the early peak of land uptake. This finding suggests that the choice of negative emission approaches is important and may affect the overall global carbon uptake (Jones et al., 2010; 2016).

Despite differences, CMIP6 ESMs agree on the amplification of the carbon cycle feedback parameters after the peaks of atmospheric CO_2 concentration and temperature. Most ESMs show that β becomes more positive and γ more negative. The increase in feedback parameters after the peaks of CO_2 concentration and temperature reflects the decreasing yet persisting carbon uptake by the ocean and land during the ramp-down phase. Both land and ocean continue to take up carbon (even though at a decreasing rate) at a rate larger than expected from linear behavior.

The amplification of carbon cycle feedback parameters influences the overall uptake by land and ocean under mitigation scenarios and thus affects the ability of the Earth System to return to the temperature target after an overshoot. We encourage future studies to investigate the consequences of amplification of feedback parameters under different overshoot pathways to understand what this means in the mitigation context and to confirm whether integrated

596 assessment models that are used for policymaking capture feature or parametrize them
597 accordingly, if necessary.

598 **Acknowledgments and Data**

599 This work benefited from the scientific contributions of several researchers, in particular,
600 Tomohiro Hajima of Japan Agency for Marine-Earth Science and Technology, Roland Séférian
601 of CNRM, and Masakazu Yoshimori of The University of Tokyo. The data from the CMIP6
602 simulations are available from the CMIP6 archive (https://esgf-node.llnl.gov/search/cmip6). Data
603 of GCB2019 are accessible via http://www.globalcarbonproject.org/carbonbudget,
604 CarbonTracker2019 via http://carbontracker.noaa.gov CAMS via
605 https://apps.ecmwf.int/datasets/data/cams-ghg-inversions/, the IIASA database via
606 https://tntcat.iiasa.ac.at/. This work was supported by the Ministère de la Transition Ecologique
607 of France through the Convention on financial support for climate services, by The Ministry of
608 Education, Culture, Sports, Science and Technology (MEXT) of Japan (Integrated Research
609 Program for Advancing Climate Models, grant no. JPMXD0717935715) and the Environment
610 Research and Technology Development Fund (JPMEERF20192004) of the Environmental
611 Restoration and Conservation Agency of Japan. K. Tanaka benefited from State assistance
612 managed by the National Research Agency in France under the “Programme d’Investissements
613 d’Avenir” under the reference “ANR-19-MPGA-0008”.

614 **Author contributions**

615 K. Tanaka conceived the research with input from O.B. and PCi. I.M. led the study, conducted
616 the analysis, and generated all figures and tables. PCa and K.Tachiiri performed additional Earth

system model simulations. I.M. and all co-authors discussed the results. I.M. drafted the manuscript, with input from all co-authors.

Conflict of Interest

The authors do not declare any competing interests.

References

Arora, V. K., Boer, G. J., Friedlingstein, P., Eby, M., Jones, C. D., Christian, J. R., et al. (2013). Carbon–Concentration and Carbon–Climate Feedbacks in CMIP5 Earth System Models. *Journal of Climate*, *26*(15), 5289–5314. https://doi.org/10.1175/JCLI-D-12-00494.1

Arora, V. K., Katavouta, A., Williams, R. G., Jones, C. D., Brovkin, V., Friedlingstein, P., et al. (2020). Carbon–concentration and carbon–climate feedbacks in CMIP6 models and their comparison to CMIP5 models. *Biogeosciences*, *17*(16), 4173–4222. https://doi.org/10.5194/bg-17-4173-2020

Boucher, O., Denvil, S., Caubel, A., & Foujols, M. A. (2018a). *IPSL IPSL-CM6A-LR model output prepared for CMIP6 CMIP piControl*. Version *20200326*. Earth System Grid Federation. doi:https://doi.org/10.22033/ESGF/CMIP6.5251

Boucher, O., Denvil, S., Caubel, A., & Foujols, M. A. (2018b). *IPSL IPSL-CM6A-LR model output prepared for CMIP6 CMIP historical*. Version *20180803*. Earth System Grid Federation. doi:https://doi.org/10.22033/ESGF/CMIP6.5195

Boucher, O., Denvil, S., Caubel, A., & Foujols, M. A. (2019a). *IPSL IPSL-CM6A-LR model output prepared for CMIP6 ScenarioMIP ssp585*. Version *20190903*. Earth System Grid Federation. doi:https://doi.org/10.22033/ESGF/CMIP6.5271

Boucher, O., Denvil, S., Caubel, A., & Foujols, M. A. (2019b). *IPSL IPSL-CM6A-LR model output prepared for CMIP6 ScenarioMIP ssp534-over*. Version *20190909*. Earth System Grid Federation. doi:https://doi.org/10.22033/ESGF/CMIP6.5269

Boucher, O., Halloran, P. R., Burke, E. J., Doutriaux-Boucher, M., Jones, C. D., Lowe, J., et al. (2012). Reversibility in an Earth System model in response to CO_2 concentration changes. *Environmental Research Letters*, *7*(2), 024013. https://doi.org/10.1088/1748-9326/7/2/024013

Boucher, O., Servonnat, J., Albright, A. L., Aumont, O., Balkanski, Y., Bastrikov, V., et al. (2020). Presentation and Evaluation of the IPSL-CM6A-LR Climate Model. *Journal of Advances in Modeling Earth Systems*, *12*(7), e2019MS002010. https://doi.org/10.1029/2019MS002010

Chevallier, F. (2013). On the parallelization of atmospheric inversions of CO_2 surface fluxes within a variational framework. *Geoscientific Model Development*, *6*(3), 783–790. https://doi.org/10.5194/gmd-6-783-2013

Ciais, P., Yao, Y., Gasser, T., Baccini, A., Wang, Y., Lauerwald, R., et al. (2020). Empirical estimates of regional carbon budgets imply reduced global soil heterotrophic respiration. *National Science Review*. https://doi.org/10.1093/nsr/nwaa145

Danabasoglu, G. (2019a). *NCAR CESM2-WACCM model output prepared for CMIP6 CMIP piControl*. Version *20190320*. Earth System Grid Federation. doi:https://doi.org/10.22033/ESGF/CMIP6.10094

Danabasoglu, G. (2019b). *NCAR CESM2-WACCM model output prepared for CMIP6 CMIP historical*. Version *20190808*. Earth System Grid Federation. doi:https://doi.org/10.22033/ESGF/CMIP6.10071

Danabasoglu, G. (2019c). *NCAR CESM2-WACCM model output prepared for CMIP6 ScenarioMIP ssp585*. Version *20200701*. Earth System Grid Federation. doi:https://doi.org/10.22033/ESGF/CMIP6.10115

Danabasoglu, G. (2019d). *NCAR CESM2-WACCM model output prepared for CMIP6 ScenarioMIP ssp534-over*. Version *20190815*. Earth System Grid Federation. doi:https://doi.org/10.22033/ESGF/CMIP6.10114

Danabasoglu, G., Lamarque, J.-F., Bacmeister, J., Bailey, D. A., DuVivier, A. K., Edwards, J., et al. (2020). The Community Earth System Model Version 2 (CESM2). *Journal of Advances in Modeling Earth Systems*, *12*(2), e2019MS001916. https://doi.org/10.1029/2019MS001916

Denvil-Sommer, A., Gehlen, M., Vrac, M., and Mejia, C. (2019) LSCE-FFNN-v1: a two-step neural network model for the reconstruction of surface ocean pCO2 over the global ocean, Geosci. Model Dev., 12, 2091–2105, https://doi.org/10.5194/gmd-12-2091-2019,

Eyring, V., Bony, S., Meehl, G. A., Senior, C. A., Stevens, B., Stouffer, R. J., & Taylor, K. E. (2016). Overview of the Coupled Model Intercomparison Project Phase 6 (CMIP6) experimental design and organization. *Geoscientific Model Development*, *9*(5), 1937. https://doi.org/10.5194/gmd-9-1937-2016

Friedlingstein, P., Cox, P., Betts, R., Bopp, L., von Bloh, W., Brovkin, V., Cadule, P., Doney, et al. (2006). Climate–Carbon Cycle Feedback Analysis: Results from the C4MIP Model Intercomparison. *Journal of Climate*, *19*(14), 3337–3353. https://doi.org/10.1175/JCLI3800.1

Friedlingstein, P., Jones, M. W., O'Sullivan, M., Andrew, R. M., Hauck, J., Peters, G. P., Peters, W., Pongratz, J., et al. (2019). Global Carbon Budget 2019. *Earth System Science Data*, *11*(4), 1783–1838. https://doi.org/10.5194/essd-11-1783-2019

Gasser, T., & Ciais, P. (2013). A theoretical framework for the net land-to-atmosphere CO_2 flux and its implications in the definition of "emissions from land-use change." *Earth System Dynamics*, *4*(1), 171–186. https://doi.org/10.5194/esd-4-171-2013

Gasser T., Kechiar M, Ciais P, Burke EJ, Kleinen T, Zhu D, Huang Y, Ekici A, et al. (2018). Path-dependent reductions in CO_2 emission budgets caused by permafrost carbon release. *Nature Geoscience* 11: 830-835. DOI:10.1038/s41561-018-0227-0

Good, P., Sellar, A., Tang, Y., Rumbold, S., Ellis, R., Kelley, D., & Kuhlbrodt, T. (2019a). *MOHC UKESM1.0-LL model output prepared for CMIP6 ScenarioMIP ssp585*. Version *20191121*. Earth System Grid Federation. doi:https://doi.org/10.22033/ESGF/CMIP6.6405

Good, P., Sellar, A., Tang, Y., Rumbold, S., Ellis, R., Kelley, D., & Kuhlbrodt, T. (2019b). *MOHC UKESM1.0-LL model output prepared for CMIP6 ScenarioMIP ssp534-over*. Version *20200415*. Earth System Grid Federation. doi:https://doi.org/10.22033/ESGF/CMIP6.6397

Gregory, J. M., Jones, C. D., Cadule, P., & Friedlingstein, P. (2009). Quantifying Carbon Cycle Feedbacks. *Journal of Climate*, *22*(19), 5232–5250. https://doi.org/10.1175/2009JCLI2949.1

Gruber, N., Clement, D., Carter, B. R., Feely, R. A., Heuven, S. van, Hoppema, M., et al. (2019). The oceanic sink for anthropogenic CO_2 from 1994 to 2007. *Science*, *363*(6432), 1193–1199. https://doi.org/10.1126/science.aau5153

Hajima, T., Abe, M., Arakawa, O., Suzuki, T., Komuro, Y., Ogura, T., Ogochi, K., Watanabe, M., et al. (2019a). *MIROC MIROC-ES2L model output prepared for CMIP6 CMIP piControl*. Version *20200124*. Earth System Grid Federation. doi:https://doi.org/10.22033/ESGF/CMIP6.5710

Hajima, T., Abe, M., Arakawa, O., Suzuki, T., Komuro, Y., Ogura, T., Ogochi, K., Watanabe, M., et al. (2019b). *MIROC MIROC-ES2L model output prepared for CMIP6 CMIP historical*.

Version *20200124*. Earth System Grid Federation.
doi:https://doi.org/10.22033/ESGF/CMIP6.5602

Hajima, T., Abe, M., Arakawa, O., Suzuki, T., Komuro, Y., Ogura, T., Ogochi, K., Watanabe, M., et al. (2020a). *MIROC MIROC-ES2L model output prepared for CMIP6 CMIP esm-piControl*. Version *20200428*. Earth System Grid Federation.
doi:https://doi.org/10.22033/ESGF/CMIP6.5512

Hajima, T., Abe, M., Arakawa, O., Suzuki, T., Komuro, Y., Ogura, T., Ogochi, K., Watanabe, M., et al. (2020b). *MIROC MIROC-ES2L model output prepared for CMIP6 CMIP esm-hist*. Version *20200318*. Earth System Grid Federation.
doi:https://doi.org/10.22033/ESGF/CMIP6.5496

Hajima, T., Abe, M., Arakawa, O., Suzuki, T., Komuro, Y., Ogura, T., Ogochi, K., Watanabe, M., et al. (2020c). *MIROC MIROC-ES2L model output prepared for CMIP6 CDRMIP esm-ssp534-over*. Version *20201106*. Earth System Grid Federation.
doi:https://doi.org/10.22033/ESGF/CMIP6.5525

Hajima, T., Kawamiya, M., Tachiiri, K., Abe, M., Arakawa, O., Suzuki, T., Komuro, Y., Ogochi, K., et al. (2019c). *MIROC MIROC-ES2L model output prepared for CMIP6 C4MIP hist-bgc*. Version *20200903*. Earth System Grid Federation.
doi:https://doi.org/10.22033/ESGF/CMIP6.5582

Hajima, T., Kawamiya, M., Tachiiri, K., Abe, M., Arakawa, O., Suzuki, T., Komuro, Y., Ogochi, K., et al. (2019d). *MIROC MIROC-ES2L model output prepared for CMIP6 C4MIP ssp534-over-bgc*. Version *20200124*. Earth System Grid Federation.
doi:https://doi.org/10.22033/ESGF/CMIP6.5769

Hajima, T., Watanabe, M., Yamamoto, A., Tatebe, H., Noguchi, M. A., Abe, M., Ohgaito, R., Ito, A., et al. (2020). Development of the MIROC-ES2L Earth system model and the evaluation of biogeochemical processes and feedbacks. *Geoscientific Model Development*, *13*(5), 2197–2244. https://doi.org/10.5194/gmd-13-2197-2020

Hausfather, Z., & Peters, G. P. (2020). Emissions – the 'business as usual' story is misleading. *Nature*, *577*(7792), 618–620. https://doi.org/10.1038/d41586-020-00177-3

Höhne, N., Elzen, M. den, Rogelj, J., Metz, B., Fransen, T., Kuramochi, T., Olhoff, A., Alcamo, J., et al. (2020). Emissions: world has four times the work or one-third of the time. *Nature*, *579*(7797), 25–28. https://doi.org/10.1038/d41586-020-00571-x

Huntzinger, D. N., Michalak, A. M., Schwalm, C., Ciais, P., King, A. W., Fang, Y., Schaefer, K., Wei, Y., et al. (2017). Uncertainty in the response of terrestrial carbon sink to environmental drivers undermines carbon-climate feedback predictions. *Scientific Reports*, *7*(1), 4765. https://doi.org/10.1038/s41598-017-03818-2

Hurtt, G. C., Chini, L., Sahajpal, R., Frolking, S., Bodirsky, B. L., Calvin, K., Doelman, J.C., Fisk, J., et al. (2020). Harmonization of Global Land-Use Change and Management for the Period 850–2100 (LUH2) for CMIP6. *Geoscientific Model Development Discussions*, 1–65. https://doi.org/10.5194/gmd-2019-360

Jacobson, A. R., Schuldt, K. N., Miller, J. B., Oda, T., Tans, P., Andrews, A., Mund, J., Ott, L., et al. (2020). CarbonTracker CT2019. https://doi.org/10.25925/39M3-6069

Jeltsch-Thömmes, A., Stocker, T. F., & Joos, F. (2020). Hysteresis of the Earth system under positive and negative CO_2 emissions. *Environmental Research Letters*. https://doi.org/10.1088/1748-9326/abc4af

748 Jones, C. (2019a). *MOHC UKESM1.0-LL model output prepared for CMIP6 C4MIP hist-bgc*.
749 Version *20200501*. Earth System Grid Federation.
750 doi:https://doi.org/10.22033/ESGF/CMIP6.6055
751 Jones, C. (2019b). *MOHC UKESM1.0-LL model output prepared for CMIP6 C4MIP ssp585-*
752 *bgc*. Version *20200714*. Earth System Grid Federation.
753 doi:https://doi.org/10.22033/ESGF/CMIP6.6409
754 Jones, C. (2020). *MOHC UKESM1.0-LL model output prepared for CMIP6 C4MIP ssp534-over-*
755 *bgc*. Version *20200501*. Earth System Grid Federation.
756 doi:https://doi.org/10.22033/ESGF/CMIP6.6401
757 Jones, C. D., Arora, V., Friedlingstein, P., Bopp, L., Brovkin, V., Dunne, J., Graven, H.,
758 Hoffman, F., et al. (2016b). C4MIP – The Coupled Climate–Carbon Cycle Model
759 Intercomparison Project: experimental protocol for CMIP6. *Geoscientific Model Development*,
760 *9*(8), 2853–2880. https://doi.org/10.5194/gmd-9-2853-2016
761 IPCC (Intergov. Panel Clim. Change). (2018). Global Warming of 1.5° C. An IPCC Special
762 Report on the Impacts of Global Warming of 1.5° C Above Pre-Industrial Levels and Related
763 Global Greenhouse Gas Emission Pathways, in the Context of Strengthening the Global
764 Response to the Threat of Climate Change, Sustainable Development, and Efforts to Eradicate
765 Poverty.
766 Jones, C.D., Ciais, P., Davis, S.J., Friedlingstein, P., Gasser, T., Peters, G.P., Rogelj, J., van
767 Vuuren D.P., et al. (2016a). Simulating the Earth system response to negative emissions.
768 Environmental Research Letters, 11(9), 095012.

769 Jones, C. D., & Friedlingstein, P. (2020). Quantifying process-level uncertainty contributions to
770 TCRE and carbon budgets for meeting Paris Agreement climate targets. *Environmental Research*
771 *Letters*, *15*(7), 074019. https://doi.org/10.1088/1748-9326/ab858a
772 Jones, C. D, Liddicoat, S. & Lowe, J. (2010) Role of terrestrial ecosystems in determining CO2
773 stabilization and recovery behaviour, Tellus B: Chemical and Physical Meteorology, 62:5, 682-
774 699, DOI: 10.1111/j.1600-0889.2010.00490.x
775 Jones, C., Liddicoat, S., Wiltshire, A. (2020). *MOHC UKESM1.0-LL model output prepared for*
776 *CMIP6 CDRMIP esm-ssp534-over*. Version *20200326*. Earth System Grid Federation.
777 doi:https://doi.org/10.22033/ESGF/CMIP6.12203
778 Khatiwala, S., Primeau, F., & Hall, T. (2009). Reconstruction of the history of anthropogenic CO
779 2 concentrations in the ocean. *Nature*, *462*(7271), 346–349. https://doi.org/10.1038/nature08526
780 Landschützer, P., Gruber, N., and Bakker, D. C. E. (2016) Decadal variations and trends of the
781 global ocean carbon sink, *Global Biogeochem. Cy.*, 30, 1396–1417,
782 https://doi.org/10.1002/2015GB005359
783 Mallapaty, S. (2020). How China could be carbon neutral by mid-century. *Nature*, *586*(7830),
784 482–483. https://doi.org/10.1038/d41586-020-02927-9
785 Meinshausen, M., Nicholls, Z. R. J., Lewis, J., Gidden, M. J., Vogel, E., Freund, M., Beyerle, U.,
786 Gessner, C., et al. (2020). The shared socio-economic pathway (SSP) greenhouse gas
787 concentrations and their extensions to 2500. *Geoscientific Model Development*, *13*(8), 3571–
788 3605. https://doi.org/10.5194/gmd-13-3571-2020
789 Meinshausen, M., E. Vogel, A. Nauels, K. Lorbacher, N. Meinshausen, D. Etheridge, P. Fraser,
790 S.A. Montzka, et al. (2016), Historical greenhouse gas concentrations, doi:10.5194/gmd-2016-
791 169

McKinley, G. A., Fay, A. R., Eddebbar, Y. A., Gloege, L., & Lovenduski, N. S. (2020). External forcing explains recent decadal variability of the ocean carbon sink. *AGU Advances,* 1, e2019AV000149. https://doi.org/10.1029/2019AV000149

O'Neill, B. C., Kriegler, E., Riahi, K., Ebi, K. L., Hallegatte, S., Carter, T. R., Mathur, R. & van Vuuren, D.P., (2014). A new scenario framework for climate change research: the concept of shared socioeconomic pathways. *Climatic Change*, *122*(3), 387–400. https://doi.org/10.1007/s10584-013-0905-2

O'Neill, B. C., Kriegler, E., Ebi, K. L., Kemp-Benedict, E., Riahi, K., Rothman, D. S., van Ruijven, B.J., van Vuuren, D.P., et al. (2017). The roads ahead: Narratives for shared socioeconomic pathways describing world futures in the 21st century. *Global Environmental Change*, *42*, 169–180. https://doi.org/10.1016/j.gloenvcha.2015.01.004

Palter, J. B., Frölicher, T. L., Paynter, D., & John, J. G. (2018). Climate, ocean circulation, and sea level changes under stabilization and overshoot pathways to 1.5 K warming. *Earth System Dynamics*, *9*(2), 817–828. https://doi.org/10.5194/esd-9-817-2018

Rödenbeck, C., Bakker, D. C. E., Metzl, N., Olsen, A., Sabine, C., Cassar, N., Reum, F., Keeling, R. F., & Heimann, M. (2014) Interannual sea–air CO_2 flux variability from an observation-driven ocean mixed-layer scheme, *Biogeosciences*, 11, 4599-4613.

Schwalm, C. R., Glendon, S., & Duffy, P. B. (2020). RCP8.5 tracks cumulative CO_2 emissions. *Proceedings of the National Academy of Sciences*, *117*(33), 19656–19657. https://doi.org/10.1073/pnas.2007117117

Schwinger, J., & Tjiputra, J. (2018). Ocean Carbon Cycle Feedbacks Under Negative Emissions. *Geophysical Research Letters*, *45*(10), 5062–5070. https://doi.org/10.1029/2018GL077790

Séférian, R., Nabat, P., Michou, M., Saint-Martin, D., Voldoire, A., Colin, J., Decharme, B., Delire, C., et al. (2019). Evaluation of CNRM Earth System Model, CNRM-ESM2-1: Role of Earth System Processes in Present-Day and Future Climate. *Journal of Advances in Modeling Earth Systems*, *11*(12), 4182–4227. https://doi.org/10.1029/2019MS001791

Séférian, R. (2018a). *CNRM-CERFACS CNRM-ESM2-1 model output prepared for CMIP6 CMIP piControl*. Version *20181115*. Earth System Grid Federation. doi:https://doi.org/10.22033/ESGF/CMIP6.4165

Séférian, R. (2018b). *CNRM-CERFACS CNRM-ESM2-1 model output prepared for CMIP6 CMIP historical*. Version *20190125*. Earth System Grid Federation. doi:https://doi.org/10.22033/ESGF/CMIP6.4068

Séférian, R.(2019a). *CNRM-CERFACS CNRM-ESM2-1 model output prepared for CMIP6 C4MIP hist-bgc*. Version *20190711*. Earth System Grid Federation. doi:https://doi.org/10.22033/ESGF/CMIP6.4047

Séférian, R. (2019b). *CNRM-CERFACS CNRM-ESM2-1 model output prepared for CMIP6 C4MIP ssp534-over-bgc*. Version *20190711*. Earth System Grid Federation. doi:https://doi.org/10.22033/ESGF/CMIP6.4223

Séférian, R., Berthet, S., Yool, A., Palmiéri, J., Bopp, L., Tagliabue, A., Kwiatkowski, L., Aumont, O., et al. (2020). Tracking Improvement in Simulated Marine Biogeochemistry Between CMIP5 and CMIP6. *Current Climate Change Reports*, *6*(3), 95–119. https://doi.org/10.1007/s40641-020-00160-0

Séférian, R., Nabat, P., Michou, M., Saint-Martin, D., Voldoire, A., Colin, J., Decharme, B., Delire, C., et al. 2019. Evaluation of CNRM Earth System Model, CNRM-ESM2-1: Role of

836 Earth System Processes in Present-Day and Future Climate. *Journal of Advances in Modeling*
837 *Earth Systems*, 11(12), pp.4182-4227. https://doi.org/10.1029/2019MS001791
838 Sellar, A. A., Jones, C. G., Mulcahy, J. P., Tang, Y., Yool, A., Wiltshire, A., O'connor, F.M.,
839 Stringer, M., et al. (2019). UKESM1: Description and Evaluation of the U.K. Earth System
840 Model. *Journal of Advances in Modeling Earth Systems*, *11*(12), 4513–4558.
841 https://doi.org/10.1029/2019MS001739
842 Swart, N.C., Cole, J.N., Kharin, V.V., Lazare, M., Scinocca, J.F., Gillett, N.P., Anstey, J., Arora,
843 et al. (2019a). The Canadian Earth System Model version 5 (CanESM5.0.3). *Geoscientific Model*
844 *Development*, *12*(11), 4823–4873. https://doi.org/10.5194/gmd-12-4823-2019
845 Swart, N.C., Cole, J.N., Kharin, V.V., Lazare, M., Scinocca, J.F., Gillett, N.P., Anstey, J., Arora,
846 et al. (2019b). *CCCma CanESM5 model output prepared for CMIP6 CMIP piControl*. Version
847 *20190429*. Earth System Grid Federation. doi:https://doi.org/10.22033/ESGF/CMIP6.3673
848 Swart, N.C., Cole, J.N., Kharin, V.V., Lazare, M., Scinocca, J.F., Gillett, N.P., Anstey, J., Arora,
849 et al. (2019c). *CCCma CanESM5 model output prepared for CMIP6 CMIP historical*. Version
850 *20190429*. Earth System Grid Federation. doi:https://doi.org/10.22033/ESGF/CMIP6.3610
851 Swart, N.C., Cole, J.N., Kharin, V.V., Lazare, M., Scinocca, J.F., Gillett, N.P., Anstey, J., Arora,
852 et al. (2019d). *CCCma CanESM5 model output prepared for CMIP6 ScenarioMIP ssp585*.
853 Version *20190429*. Earth System Grid Federation.
854 doi:https://doi.org/10.22033/ESGF/CMIP6.3696
855 Swart, N.C., Cole, J.N., Kharin, V.V., Lazare, M., Scinocca, J.F., Gillett, N.P., Anstey, J., Arora,
856 et al. (2019e). *CCCma CanESM5 model output prepared for CMIP6 ScenarioMIP ssp534-over*.
857 Version *20190429*. Earth System Grid Federation.
858 doi:https://doi.org/10.22033/ESGF/CMIP6.3694

Swart, N.C., Cole, J.N., Kharin, V.V., Lazare, M., Scinocca, J.F., Gillett, N.P., Anstey, J., Arora, et al. (2019f). *CCCma CanESM5 model output prepared for CMIP6 C4MIP hist-bgc*. Version *20190429*. Earth System Grid Federation. doi:https://doi.org/10.22033/ESGF/CMIP6.3600

Swart, N.C., Cole, J.N., Kharin, V.V., Lazare, M., Scinocca, J.F., Gillett, N.P., Anstey, J., Arora, et al. (2019g). *CCCma CanESM5 model output prepared for CMIP6 C4MIP ssp585-bgc*. Version *20190429*. Earth System Grid Federation. doi:https://doi.org/10.22033/ESGF/CMIP6.3697

Swart, N.C., Cole, J.N., Kharin, V.V., Lazare, M., Scinocca, J.F., Gillett, N.P., Anstey, J., Arora, et al. (2019h). *CCCma CanESM5 model output prepared for CMIP6 C4MIP ssp534-over-bgc*. Version *20190429*. Earth System Grid Federation. doi:https://doi.org/10.22033/ESGF/CMIP6.3695

Tachiiri, K., Kawamiya, M. (2020). *MIROC MIROC-ES2L model output prepared for CMIP6 ScenarioMIP ssp534-over*. Version *20201014*. Earth System Grid Federation. doi:https://doi.org/10.22033/ESGF/CMIP6.5767

Tang, Y., Rumbold, S., Ellis, Kelley, D., Mulcahy, J., Sellar, A., Walton, J., Jones, C. (2019). *MOHC UKESM1.0-LL model output prepared for CMIP6 CMIP piControl*. Version *20191119*. Earth System Grid Federation. doi:https://doi.org/10.22033/ESGF/CMIP6.6298

Tang, Y., Rumbold, S., Ellis,, Kelley, D., Mulcahy, J., Sellar, A., Walton, J., Jones, C. (2019). *MOHC UKESM1.0-LL model output prepared for CMIP6 CMIP historical*. Version *20191128*. Earth System Grid Federation. doi:https://doi.org/10.22033/ESGF/CMIP6.6113

Tang, Y., Rumbold, S., Ellis, R., Kelley, D., Mulcahy, J., Sellar, A., Walton, J., Jones, C. (2019). *MOHC UKESM1.0-LL model output prepared for CMIP6 CMIP esm-piControl*. Version *20191112*. Earth System Grid Federation. doi:https://doi.org/10.22033/ESGF/CMIP6.5953

882 Tang, Y., Rumbold, S., Ellis, R., Kelley, D., Mulcahy, J., Sellar, A., Walton, J., Jones, C. (2019).
883 *MOHC UKESM1.0-LL model output prepared for CMIP6 CMIP esm-hist*. Version *20191112*.
884 Earth System Grid Federation. doi:https://doi.org/10.22033/ESGF/CMIP6.5929
885 Tebaldi, C., Debeire, K., Eyring, V., Fischer, E., Fyfe, J., Friedlingstein, P., Knutti, R., Lowe, J.,
886 et al.: Climate model projections from the Scenario Model Intercomparison Project
887 (ScenarioMIP) of CMIP6, *Earth Syst. Dynam. Discuss.*, https://doi.org/10.5194/esd-2020-68, in
888 review, 2020.
889 Tokarska, K. B., Zickfeld, K., & Rogelj, J. (2019). Path Independence of Carbon Budgets When
890 Meeting a Stringent Global Mean Temperature Target After an Overshoot. *Earth's Future*,
891 *7*(12), 1283–1295. https://doi.org/10.1029/2019EF001312
892 United Nations / Framework Convention on Climate Change (2015). FCCC/CP/2015/L.9/Rev.1:
893 Adoption of the Paris Agreement, (pp. 1–32). UNFCCC, Paris, France.
894 Voldoire, A. (2019). *CNRM-CERFACS CNRM-ESM2-1 model output prepared for CMIP6*
895 *ScenarioMIP ssp534-over*. Version *20190410*. Earth System Grid Federation.
896 doi:https://doi.org/10.22033/ESGF/CMIP6.4221
897 Williams, R.G., Katavouta, A. & Goodwin, P. Carbon-Cycle Feedbacks Operating in the Climate
898 System. Curr Clim Change Rep 5, 282–295 (2019). https://doi.org/10.1007/s40641-019-00144-9
899 Willeit, M., Ganopolski, A., Dalmonech, D., Foley, A. M., & Feulner, G. (2014). Time-scale and
900 state dependence of the carbon-cycle feedback to climate. *Climate dynamics*, 42(7-8), 1699-
901 1713.
902 Zickfeld, K., MacDougall, A. H., & Matthews, H. D. (2016). On the proportionality between
903 global temperature change and cumulative CO_2 emissions during periods of net negative CO_2

emissions. *Environmental Research Letters*, *11*(5), 055006. https://doi.org/10.1088/1748-9326/11/5/055006